

AD-A179 175

DTIC FILE COPY

AFGL-TR-86-0218

INFLUENCE OF SCATTERING ON SEISMIC WAVES

Anton M. Dainty
M. Nafi Toksöz

Earth Resources Laboratory
Department of Earth, Atmospheric, and
Planetary Sciences
Massachusetts Institute of Technology
Cambridge, Massachusetts 02139

21 October 1986

Scientific Report No. 1

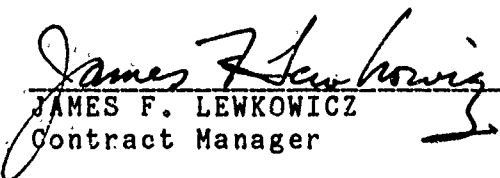
APPROVED FOR PUBLIC RELEASE; DISTRIBUTION UNLIMITED

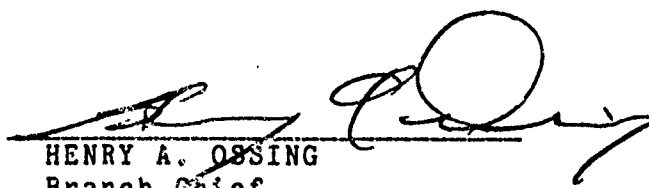
Air Force Geophysics Laboratory
Air Force Systems Command
United States Air Force
Hanscom Air Force Base, Massachusetts 01731

DTIC
ELECTE
APR 20 1987
S D
E


87 4 17 077

"This technical report has been reviewed and is approved for publication"


JAMES F. LEWKOWICZ
Contract Manager


HENRY A. OSSING
Branch Chief

FOR THE COMMANDER


DONALD H. ECKHARDT
Division Director

This report has been reviewed by the ESD Public Affairs Office (PA) and is releasable to the National Technical Information Service (NTIS).

Qualified requestors may obtain additional copies from the Defense Technical Information Center. All others should apply to the National Technical Information Service.

If your address has changed, or if you wish to be removed from the mailing list, or if the addressee is no longer employed by your organization, please notify AFGL/DAA, Hanscom AFB, MA 01731. This will assist us in maintaining a current mailing list.

Do not return copies of this report unless contractual obligations or notices on a specific document requires that it be returned.

REPORT DOCUMENTATION PAGE

1a. REPORT SECURITY CLASSIFICATION Unclassified			1b. RESTRICTIVE MARKINGS		
2a. SECURITY CLASSIFICATION AUTHORITY			3. DISTRIBUTION/AVAILABILITY OF REPORT Approved for public release; distribution unlimited		
2b. DECLASSIFICATION/DOWNGRADING SCHEDULE					
4. PERFORMING ORGANIZATION REPORT NUMBER(S)			5. MONITORING ORGANIZATION REPORT NUMBER(S) AFGL-TR-86-0218		
6a. NAME OF PERFORMING ORGANIZATION Earth Resources Laboratory Dept. of Earth, Atmospheric, and Planetary Sciences		6b. OFFICE SYMBOL (If applicable)	7a. NAME OF MONITORING ORGANIZATION Air Force Geophysics Laboratory		
6c. ADDRESS (City, State, and ZIP Code) Massachusetts Institute of Technology Cambridge, MA 02139			7b. ADDRESS (City, State, and ZIP Code) Hanscom AFB, MA 01731		
8a. NAME OF FUNDING/SPONSORING ORGANIZATION		8b. OFFICE SYMBOL (If applicable)	9. PROCUREMENT INSTRUMENT IDENTIFICATION NUMBER F19628-86-K-0004		
8c. ADDRESS (City, State, and ZIP Code)			10. SOURCE OF FUNDING NUMBERS		
			PROGRAM ELEMENT NO. 61101E	PROJECT NO. 6A10	TASK NO. DA
					WORK UNIT ACCESSION NO. BF
11. TITLE (Include Security Classification) Influence of Scattering on Seismic Waves (unclassified)					
12. PERSONAL AUTHOR(S) Anton M. Dainty, M. Nafi Toksöz					
13a. TYPE OF REPORT Scientific Report No. 1		13b. TIME COVERED FROM 2/1/86 TO 7/31/86		14. DATE OF REPORT (Year, Month, Day) 1986 October 21	
15. PAGE COUNT 42					
16. SUPPLEMENTARY NOTATION					
17. COSATI CODES			18. SUBJECT TERMS (Continue on reverse if necessary and identify by block number)		
FIELD	GROUP	SUB-GROUP	wavenumber spectrum, frequency-wavenumber spectrum, NORESS, noise, coherency, velocity bias, ultrasonic models		
19. ABSTRACT (Continue on reverse if necessary and identify by block number) Tests have been carried out to find sources of noise and velocity bias in a new array analysis method, the wavenumber spectrum, which has been used at NORESS to detect diffuse components of teleseismic coda. Noise problems have been analysed by using subarrays and identified as being due to loss of coherence between signals at sensors of given spacing as frequency increases. Velocity bias has been investigated using synthetic signals and is caused by the finite array aperture. As a result of these investigations, it is concluded that the full array should be used in the frequency range 1-2.5 Hz, the array less the outer ring for 2.5-5 Hz and the array less the two outer rings for 5-10 Hz. In addition, a preliminary report is given on the use of ultrasonic modeling to investigate coda. Keywords seismic arrays; Norway; seismic scattering; seismic noise.					
20. DISTRIBUTION/AVAILABILITY OF ABSTRACT <input checked="" type="checkbox"/> UNCLASSIFIED/UNLIMITED <input type="checkbox"/> SAME AS RPT <input type="checkbox"/> DTIC USERS			21. ABSTRACT SECURITY CLASSIFICATION unclassified		
22a. NAME OF RESPONSIBLE INDIVIDUAL James F. Lewkowicz			22b. TELEPHONE (Include Area Code) 617/377-3028		22c. OFFICE SYMBOL LWH

TABLE OF CONTENTS

REPORT DOCUMENTATION PAGE WITH ABSTRACT	i
I. INTRODUCTION	1
II. WAVENUMBER SPECTRA	2
III. ULTRASONIC MODELING	23
REFERENCES	38

Accession For		
NTIS GRA&I	<input checked="" type="checkbox"/>	
DTIC TAB	<input type="checkbox"/>	
Unannounced	<input type="checkbox"/>	
Justification		
By _____		
Distribution/		
Availability Codes		
Dist	Avail and/or Special	
A-1		



I. INTRODUCTION

Scattering phenomena occur universally for short period (frequency ≥ 1 Hz) seismic waves observed at the earth's surface. One of the major manifestations of scattering is the presence of coda, seismic energy following a major P or S arrival that cannot be explained by propagation in a layered structure. In this project coda is being examined by two methods. The first method is to use the NORESS array in southern Norway to examine telesismic, regional and local coda. In preliminary investigations carried out last year on telesismic P coda (Dainty, 1985), a promising analysis method ("wavenumber spectrum") was identified. In this report we discuss some tests that have been made to characterize certain biases and limitations of the wavenumber spectra noted in the preliminary investigation. The second method we are using is ultrasonic modeling; preliminary work on building models to produce coda in the laboratory is presented together with a discussion of some appropriate investigations that might be carried out.

The objective of the study is to understand the coda so that it may be used to estimate yield (Bullitt and Cormier, 1984; Gupta *et al.*, 1985), measure attenuation (Aki and Chouet, 1975) and as a possible discriminant between earthquakes and explosions (Dainty, 1985). At present these objectives suffer from a lack of understanding of the components that make up coda and uncertainty concerning the limits of validity of the single scattering theory used to analyse coda.

II. WAVENUMBER SPECTRA

Summary of Previous Work

The data taken at NORESS may be considered as a sampling in time and two space dimensions of a wavefield. Since harmonic waves are fundamental solutions of the wave equation, it is often useful to perform a three dimensional spectral analysis to find power as a function of frequency f and two components of (linear) wavenumber, say wavenumber North (k_N) and wavenumber East (k_E). A contour plot of such a transform at a frequency of 3.6 Hz against k_N and k_E is shown in Figure 1 for a teleseismic event shown, along with the coda analysis window used, in Figure 2. From such a plot we may begin to break down the coda into constituent parts corresponding to waves scattered in different places. Two well known criteria may be used. One uses the azimuth ϑ of a wave measured clockwise from North, given by

$$\tan \vartheta = k_E / k_N \quad (1)$$

The second criterion is to use the apparent velocity V_a given by

$$V_a = f / k \quad (2)$$

where the *total horizontal wavenumber* k is given by

$$k^2 = k_N^2 + k_E^2 \quad (3)$$

The apparent velocity V_a is related to the velocity of the surface material V_s and the angle of incidence of the wave to the vertical i by

$$V_a = V_s / \sin i \quad (4)$$

In the coda i is not in general known, and another relation from (4) must be used instead,

MONOCHROMATIC F-K ANALYSIS
CONVENTIONAL RESOLUTION
LINEAR DEPENDENCY BETWEEN CONTOURS

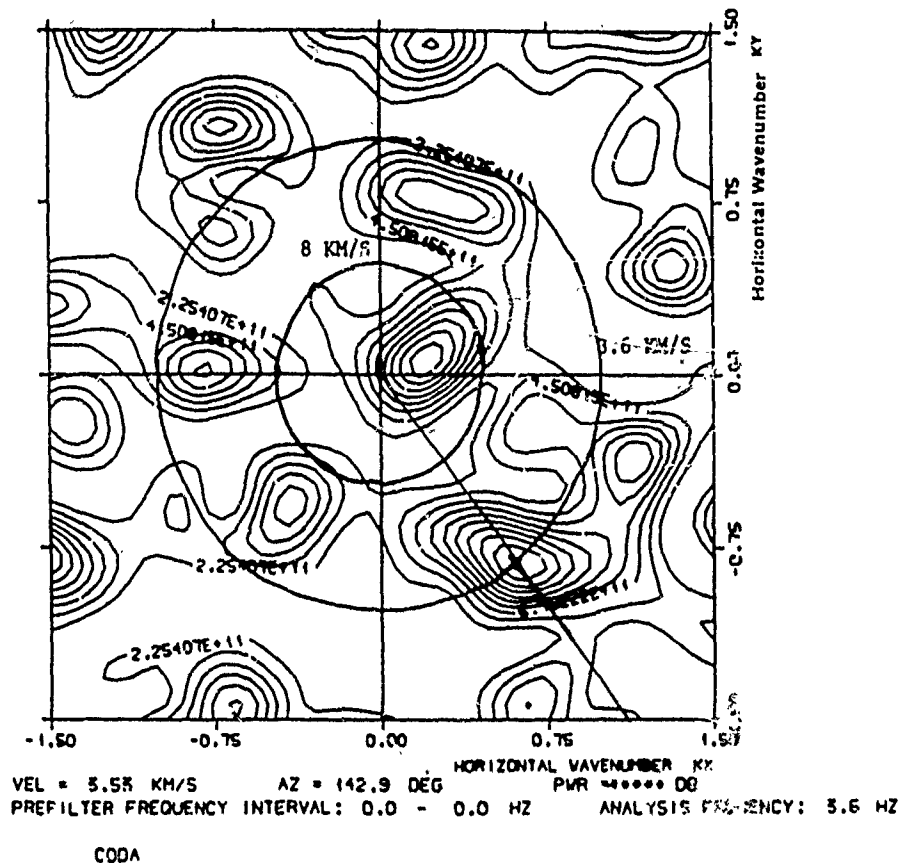


Figure 1. Frequency-wavenumber spectrum for event and window of Figure 2. Analysis frequency is 3.6 Hz, KX is wavenumber East, KY wavenumber North, units are 1/km. From Dainty (1985).

1985 FEB 10

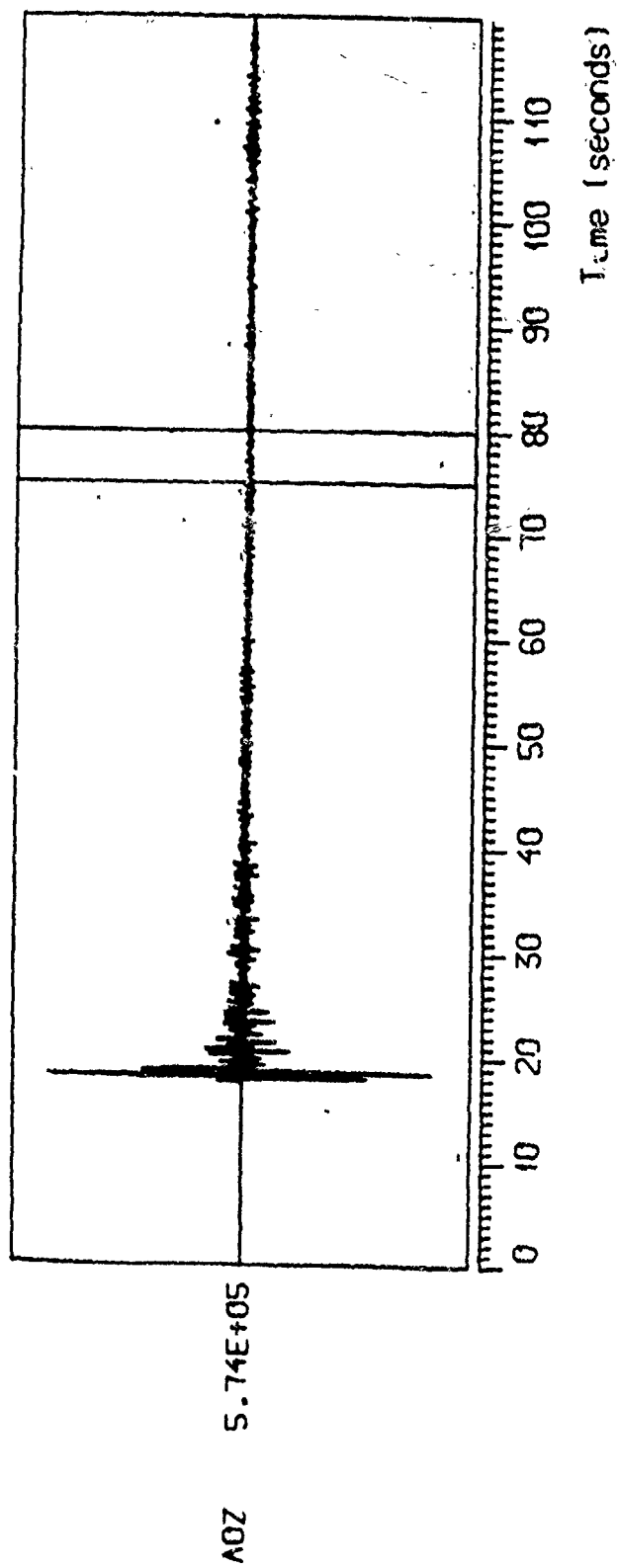


Figure 2. Teleseismic event recorded at the center seismometer, NORESS. Analysis window is shown. From Dairty (1985).

$$V_a \approx V_s$$

For investigations of coda, the interesting range of V_a is the crustal range 3 - 9 km/s; any component with an apparent velocity faster than 9 km/s may be classified as teleseismic.

From (1), (2) and (3) lines passing outwards from the origin on Figure 1 are lines of constant azimuth while circles centered on the origin are lines of constant total wavenumber and also lines of constant apparent velocity. A line of constant azimuth and two circles of constant phase velocity are shown on Figure 1; teleseismic P waves will have faster apparent velocities than 8 km/s while Lg waves will have velocities close to 3.6 km/s. In coda studies it is often useful to know the total power as a function of azimuth or total wavenumber (i.e., apparent velocity). To obtain this information the frequency-wavenumber spectrum shown in Figure 1 must be integrated along a line of constant azimuth or constant total wavenumber. Appropriate formulations for doing this will be given in a forthcoming publication. Figure 3 shows the result for azimuth and Figure 4 for wavenumber. So far, the *wavenumber spectrum* as shown in Figure 4 has been used in coda analysis.

Figure 4 illustrates some of the strengths and also one of the limitations of wavenumber spectra. Note that there are two peaks superimposed on a linear trend. The two peaks indicate that there is a preponderance of energy at two phase velocities in the signal, a high phase velocity of 18 km/s and a low phase velocity of 4.3 km/s. The high phase velocity peak may also be seen in Figure 1 (the peak inside the 8 km/s circle) where it is clear that the energy is coming in with a definite azimuth ($\sim 75^\circ$) that is in fact the source azimuth, indicating near source scattering. The high phase velocity indicates that the energy has travelled from the source as P. A comparison of Figure 4 and Figure 1 indicates that the low velocity peak is made up of the sum of several peaks with differing azimuths, none of them the source azimuth. This diffuse component of the coda is interpreted as being locally scattered within the crust near the receiver, since it has the apparent velocity of S waves incident nearly horizontally. Finding such "diffuse" com-

1985 FEB 10

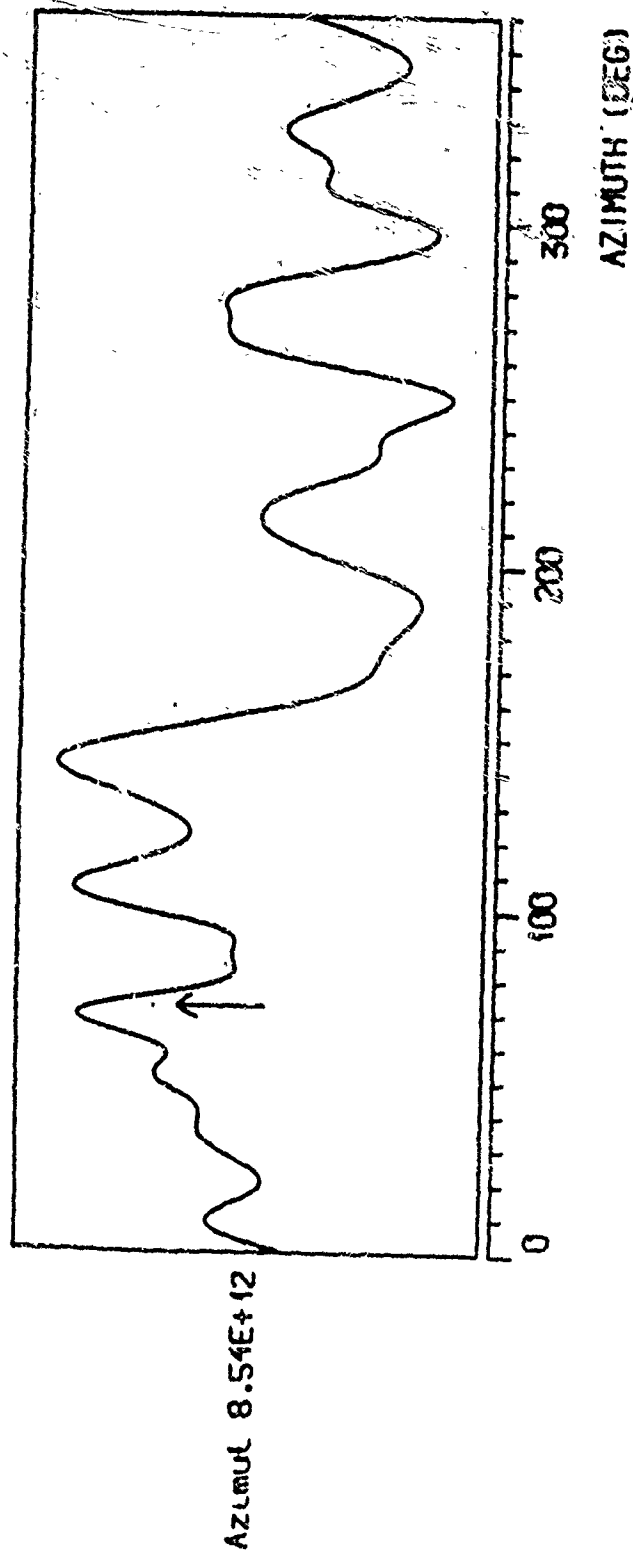


Figure 3. Azimuth spectrum of event and window of Figure 2 at a frequency of 3.6 Hz. Arrow indicates known source azimuth. From Dainty (1985).

1985 FEB 10

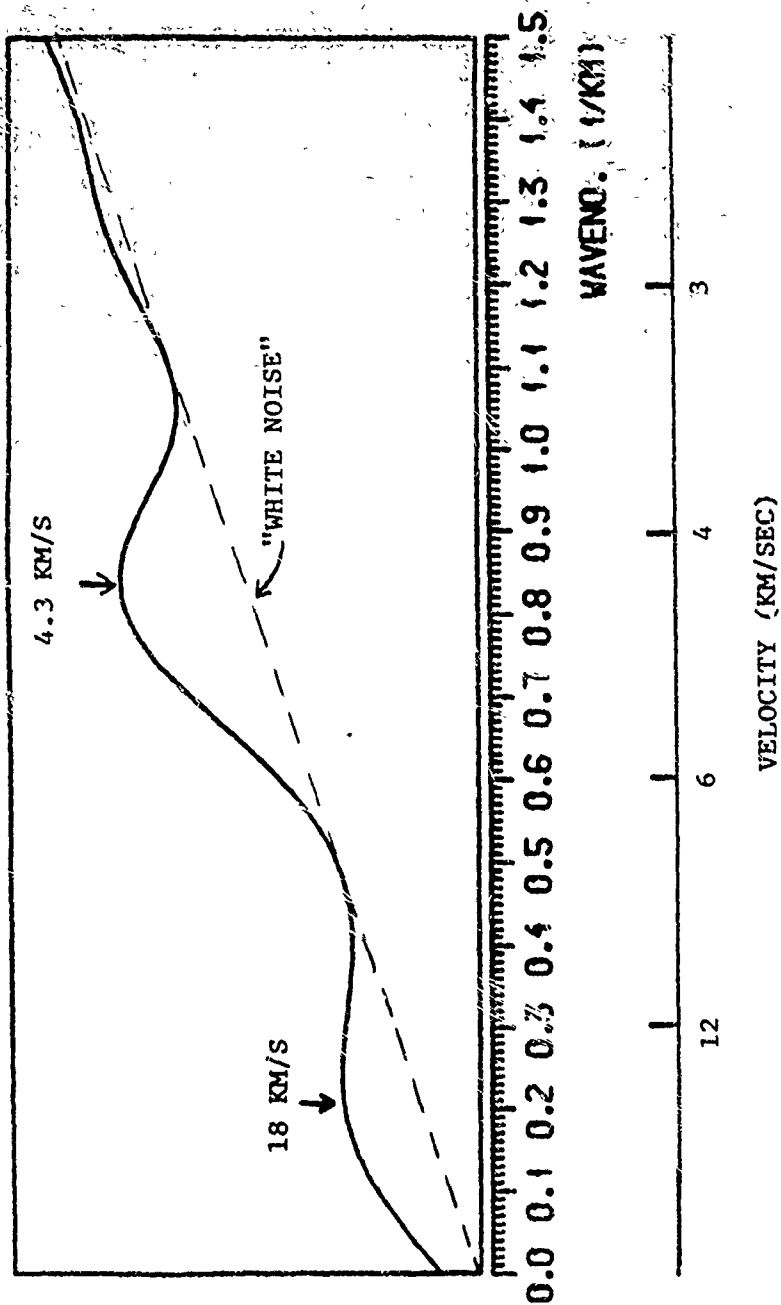


Figure 4. Wavenumber spectrum of event and window of Figure 2 at a frequency of 3.0 Hz. Velocity scale is indicated. From Dainty (1985).

ponents in the coda has been a major use of the wavenumber spectrum.

One of the difficulties encountered in the use of wavenumber spectra has been the presence of linear trends such as that labelled "white noise" in Figure 4. The term is used because a constant ("white noise") frequency-wavenumber spectrum will produce such a trend due to the increasing circumference of the circle of integration as the total wavenumber increases. This problem increases with increasing frequency if the full array is used. Another problem shows up at low frequencies as illustrated by Figures 5 and 6, which present analyses of the event shown in Figure 2 but at 1.6 - 1.8 Hz instead of 3.6 Hz. Figure 5 shows the frequency-wavenumber spectra for a window around first P and for the coda 20 - 100 sec after first P. Both show a prominent peak with the source azimuth and a high apparent velocity - 15.5 km/s for first P and 11.7 km/s for the coda. The wavenumber spectrum for the same two windows is shown in Figure 6. The first P window shows a single major peak but the peak is at a lower apparent velocity (9 km/s) than the peak in Figure 5, i.e., there is a bias in the apparent velocity determined from the wavenumber spectrum. The coda wavenumber spectrum has been interpreted as consisting of two peaks (Dainty, 1985) as indicated in Figure 6. The peak with the higher apparent velocity is interpreted as corresponding to the peak in Figure 5, but again there is a bias towards a lower apparent velocity (7.2 km/s). The other peak corresponds to the diffuse local component of the coda and is not evident in Figure 5, presumably because of the spread in azimuth.

Coherence and Bias in Wavenumber Spectra

The two problems noted above may be explained by the known characteristics of the array and seismic signals received at it. In this section we present some work on the use of subarrays to minimise the "white noise" linear trends observed at high frequencies, and work on the use of synthetic signals to quantify the apparent velocity bias observed at low frequencies.

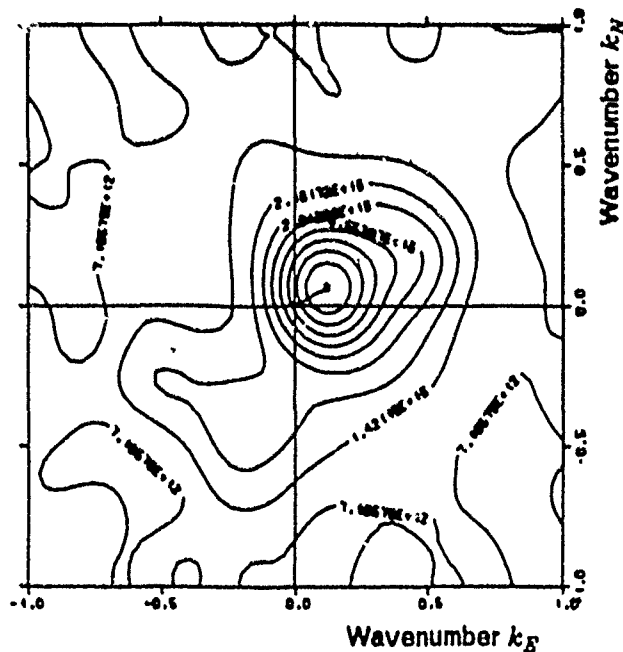
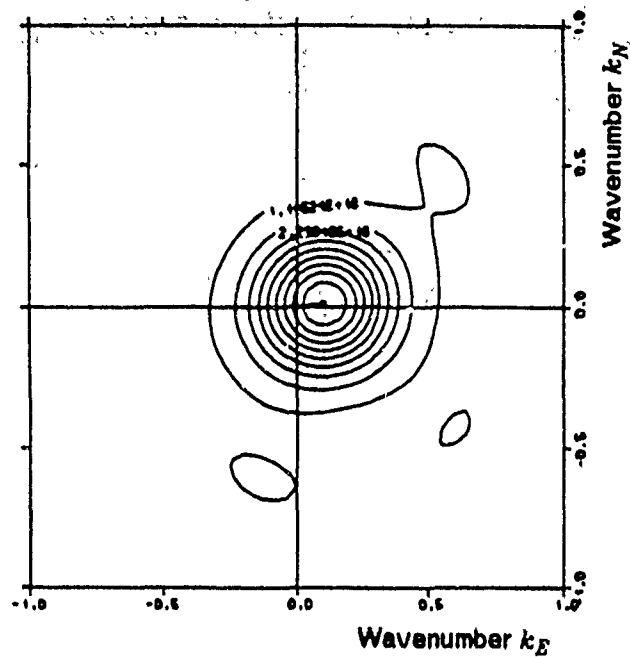


Figure 5. Frequency-wavenumber spectra of the event shown in Figure 2 at a frequency of 1.6 Hz. (Top) Five second window around first P. (Bottom) Window between 20 and 100 seconds after first P (coda), calculated as average of non-overlapping 5 second windows. From Dainty (1985).

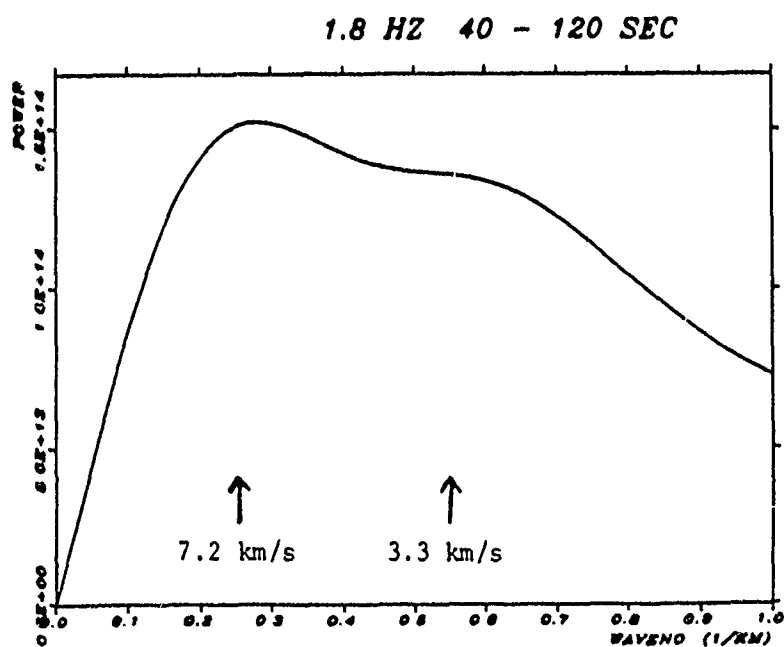
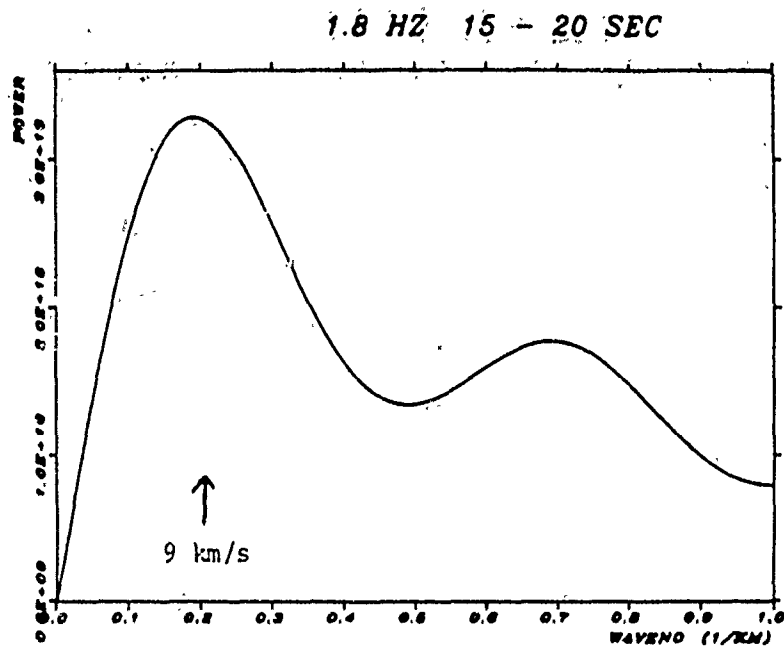


Figure 6. Wavenumber spectra of the event shown in Figure 2 at a frequency of 1.8 Hz. Windows as for Figure 5. From Dainty (1985).

One possible explanation for the white noise phenomenon is a lack of correlation of the signal at different seismometers of the array. Uncorrelated signals would appear as white noise on a wavenumber spectrum because they cannot be expressed as travelling waves. Such a lack of correlation at distances comparable to the inter-seismometer spacing has been observed in studies of noise at NORESS. Figure 7 from Bungum *et al.* (1985) shows noise correlation against distance for the NORESS site for four frequency bands. If the noise can be considered to be a wavefield consisting of a mixture of travelling waves, the results will also apply to seismic signals, especially in the coda. From Figure 7, at a fixed seismometer separation, 500 m say, the correlation declines with increasing frequency. A map of the NORESS array is shown in Figure 8, and it may be seen that the outermost ring of seismometers has a minimum separation of about 500 m from other array locations. From Figure 7 a deterioration of the wavenumber spectrum at frequencies greater than 2 Hz would be expected if the outer ring is used; this is observed. The effect should be more pronounced at higher frequencies; this also is observed.

If this is in fact the cause of the white noise problem, it should be possible to mitigate it by eliminating from the calculation of the wavenumber spectrum array elements that are far from all other array elements. Tests have been made of subarrays from which the outer ring has been eliminated and from which the two outer rings have been eliminated (Figure 8). Figure 9 shows the seismogram at the center seismometer for a local quarry blast south of NORESS with an analysis window around first P indicated. Figures 10 - 15 are frequency-wavenumber and wavenumber spectra for, in order, the full array (taken at 7.2 Hz, close to the peak signal frequency), the array minus the outer ring (subarray A), and the array minus the outer two rings (subarray B). While the frequency-wavenumber spectrum using the full array (Figure 10) does pick out the appropriate azimuth and phase velocity of the arrival, the wavenumber spectrum (Figure 11) is heavily contaminated with noise, although there is a peak at the correct wavenumber (1 km^{-1}). The results for subarray A (Figures 12 and 13) and subarray B (Figures 14 and 15) have considerably less noise, but besides a peak at the expected wavenumber of 1 km^{-1} subarray A shows a peak

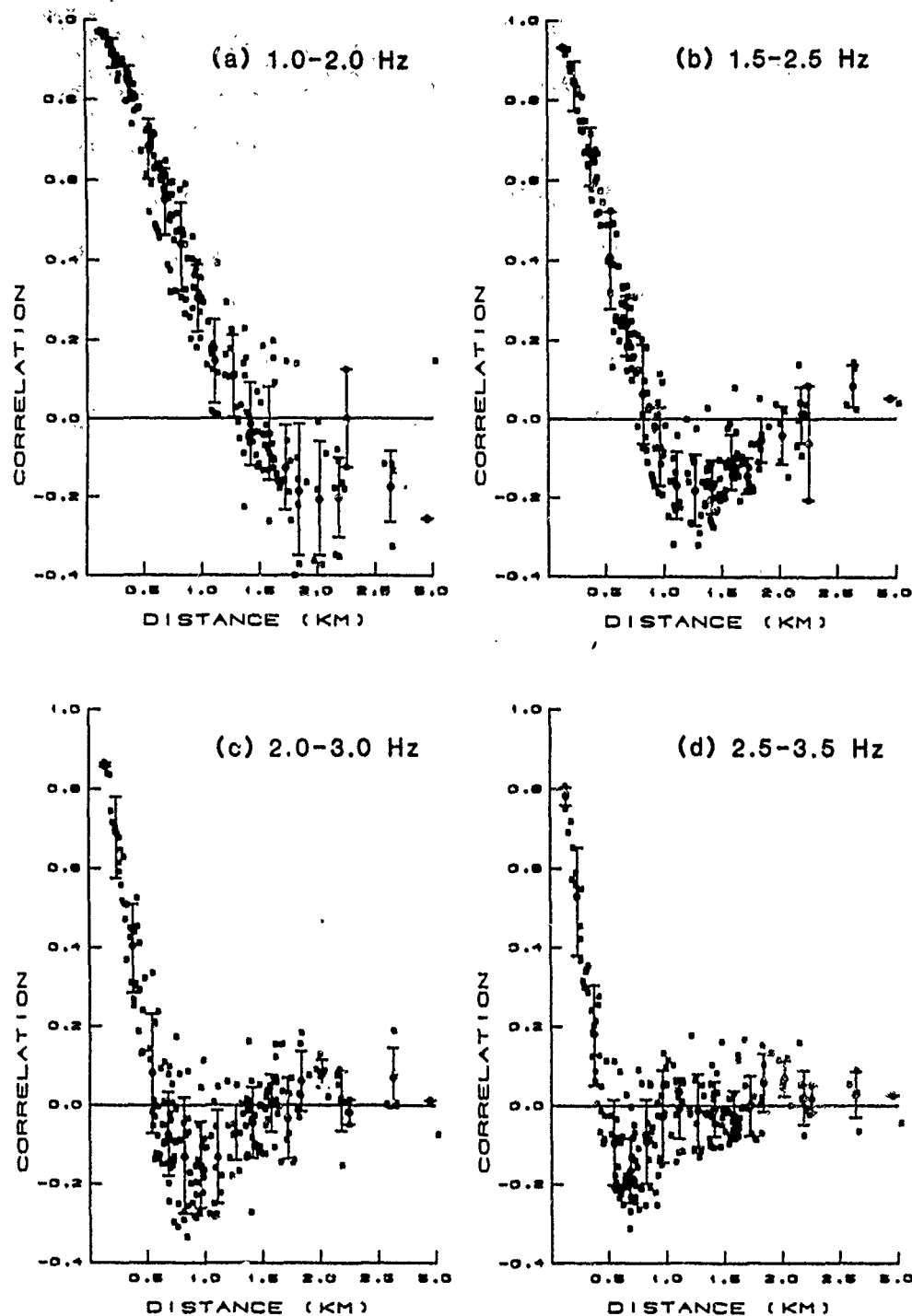


Figure 7. Observed correlation of noise between array sensors as a function of distance between them taken using a temporary NORESS array of 21 seismometers. Data was collected on August 12, 1983. Frequency band analysed is shown on each plot; all plots use the same data. From Bungum *et al.* (1985).

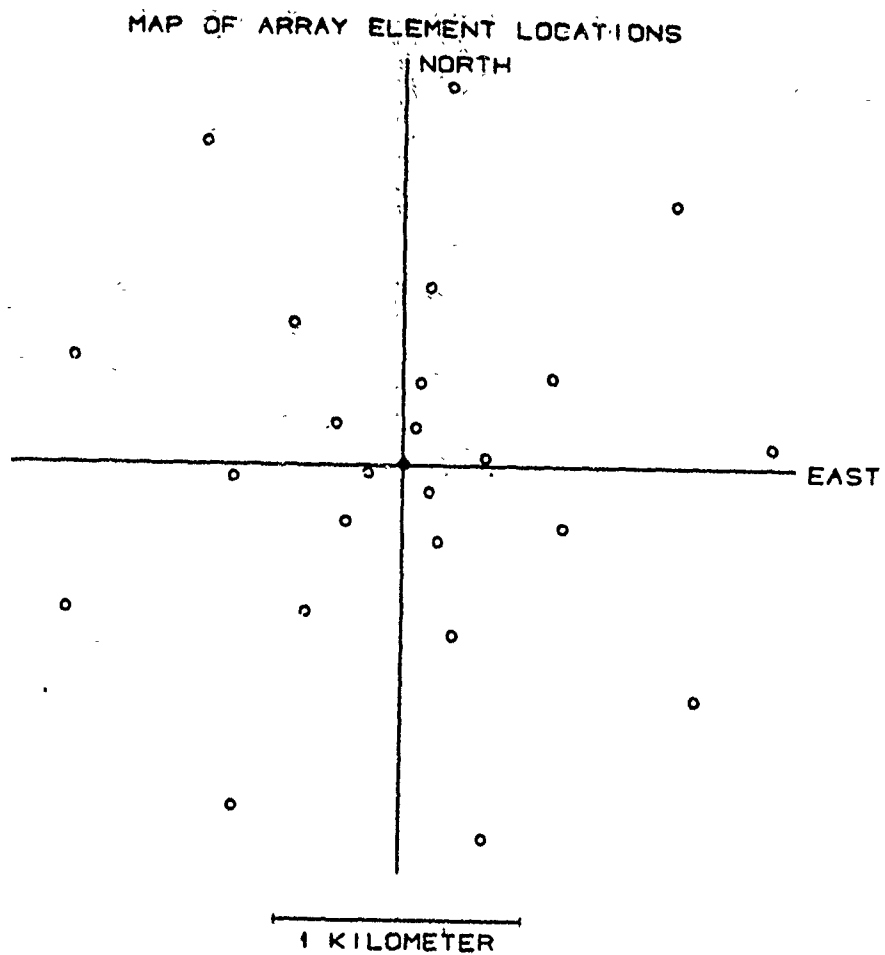


Figure 8. Map of NORESS array seismometer sites.

Stack plot

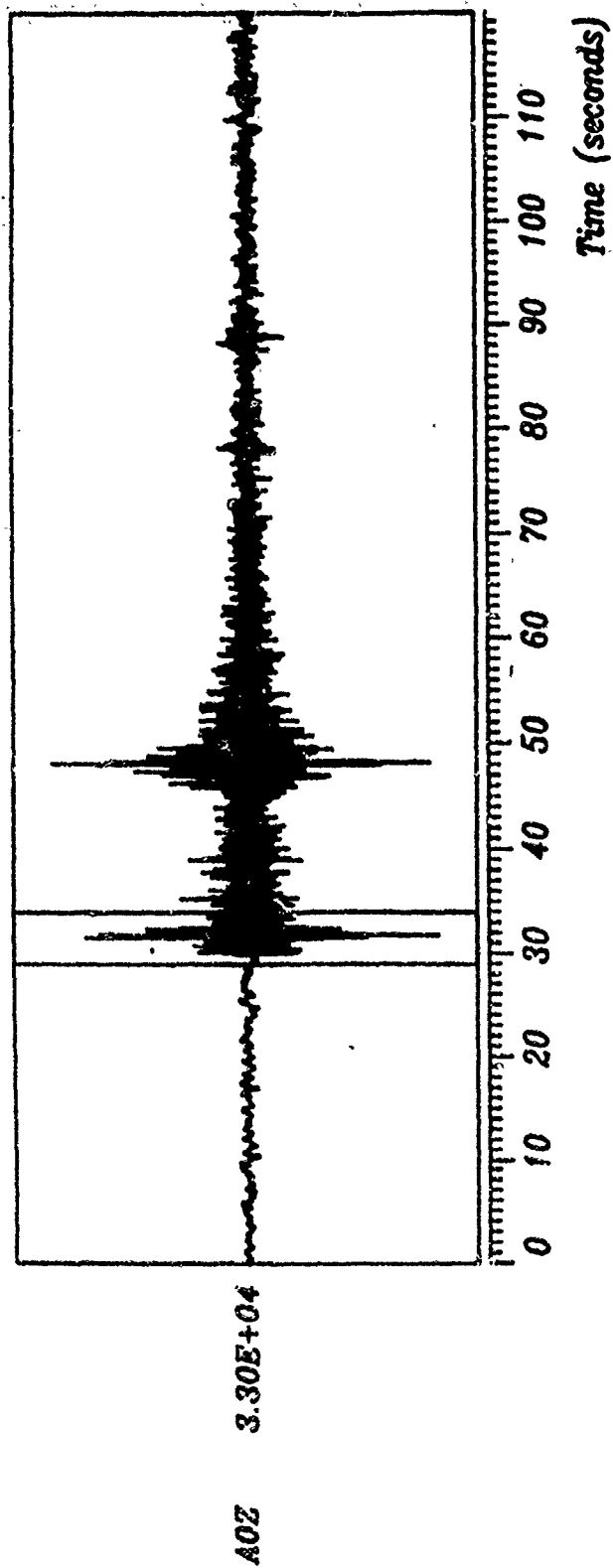


Figure 9. Local quarry blast south of NORESS recorded at the center seismometer of the array. Analysis window indicated.

MONOCHROMATIC F-K ANALYSIS
CONVENTIONAL RESOLUTION
LINEAR DEPENDENCY BETWEEN CONTOURS

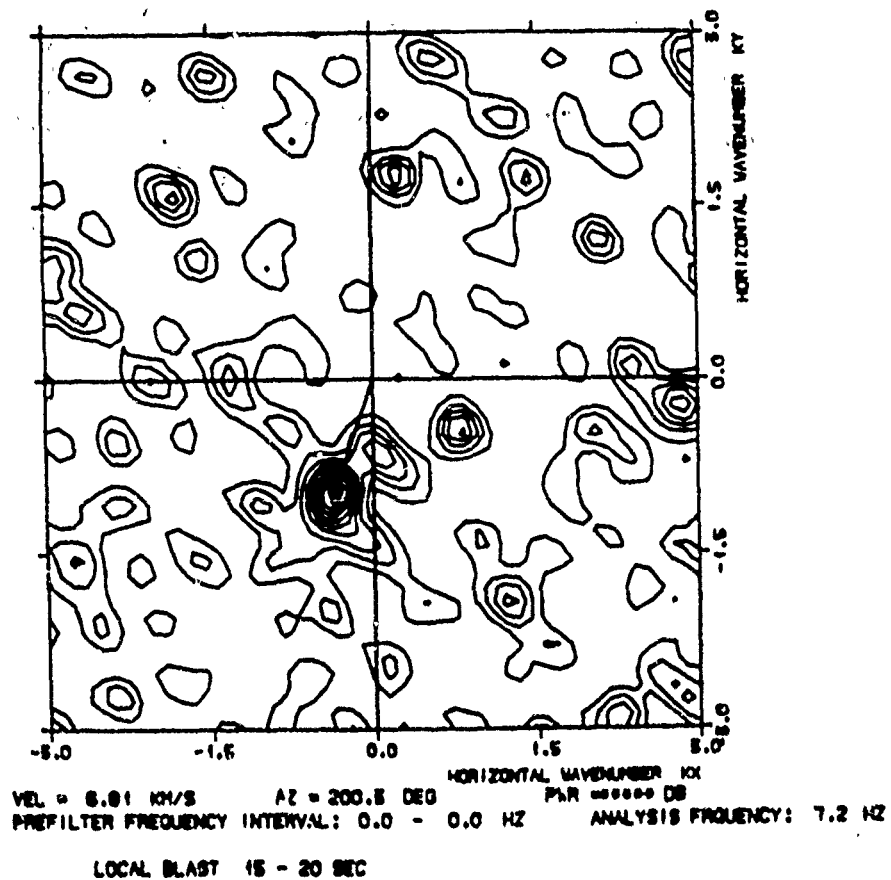


Figure 10. Frequency-wavenumber spectrum of event and window of Figure 9 at a frequency of 7.2 Hz using the full array.

LOCAL BLAST 7.2 HZ 15 - 20 SEC

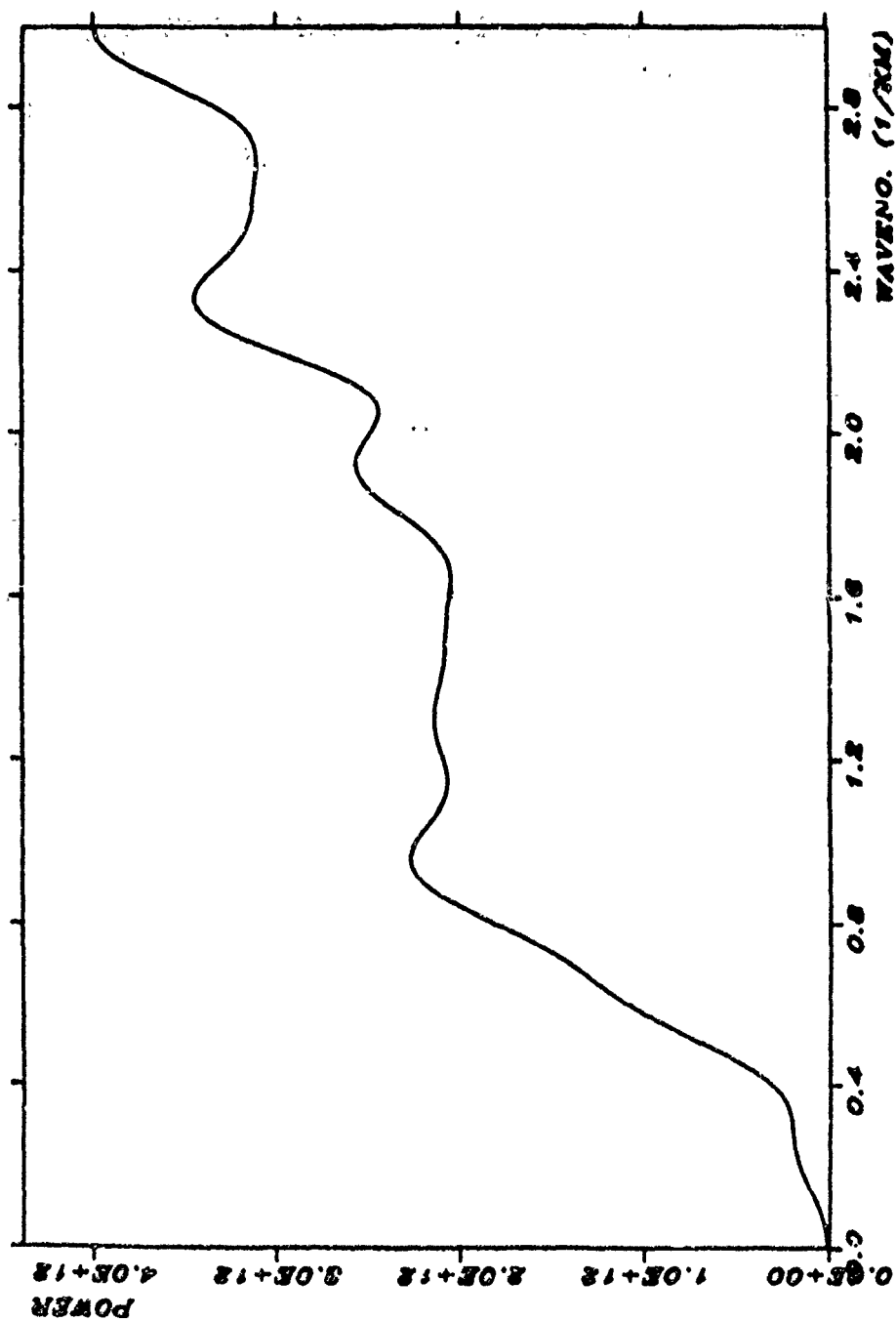


Figure 11. Wavenumber spectrum of event and window of Figure 9 at a frequency of 7.2 Hz using the full array.

MONOCHROMATIC F-K ANALYSIS
CONVENTIONAL RESOLUTION
LINEAR DEPENDENCE BETWEEN CONTOURS.

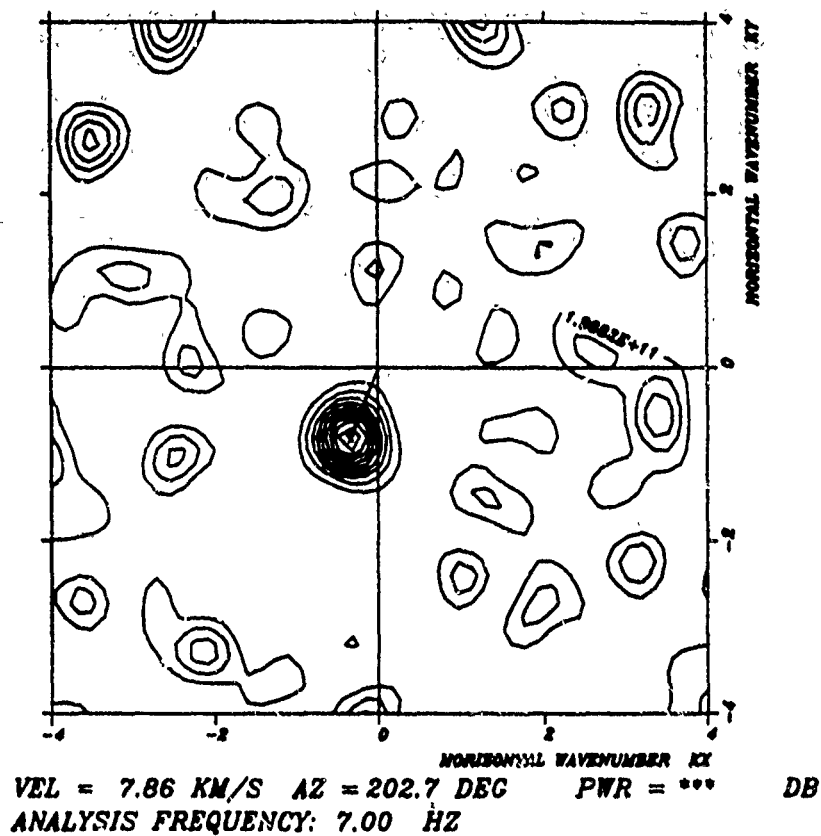


Figure 12. Frequency-wavenumber spectrum of event and window of Figure 9 at a frequency of 7.2 Hz using subarray A.

Stack plot

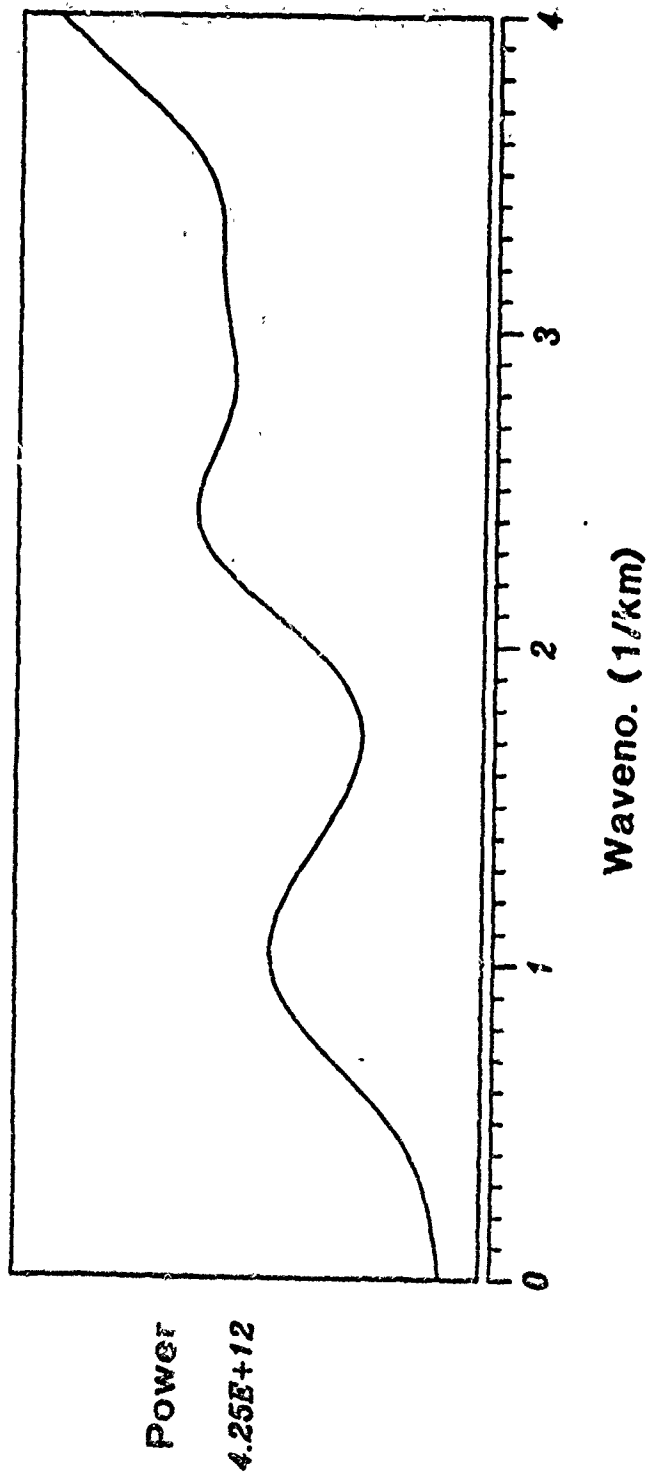


Figure 12. Wavenumber spectrum of event and window of Figure 9 at a frequency of 7.2 Hz using subarray A.

MONOCHROMATIC F-K ANALYSIS
CONVENTIONAL RESOLUTION
LINEAR DEPENDENCY BETWEEN CONTOURS

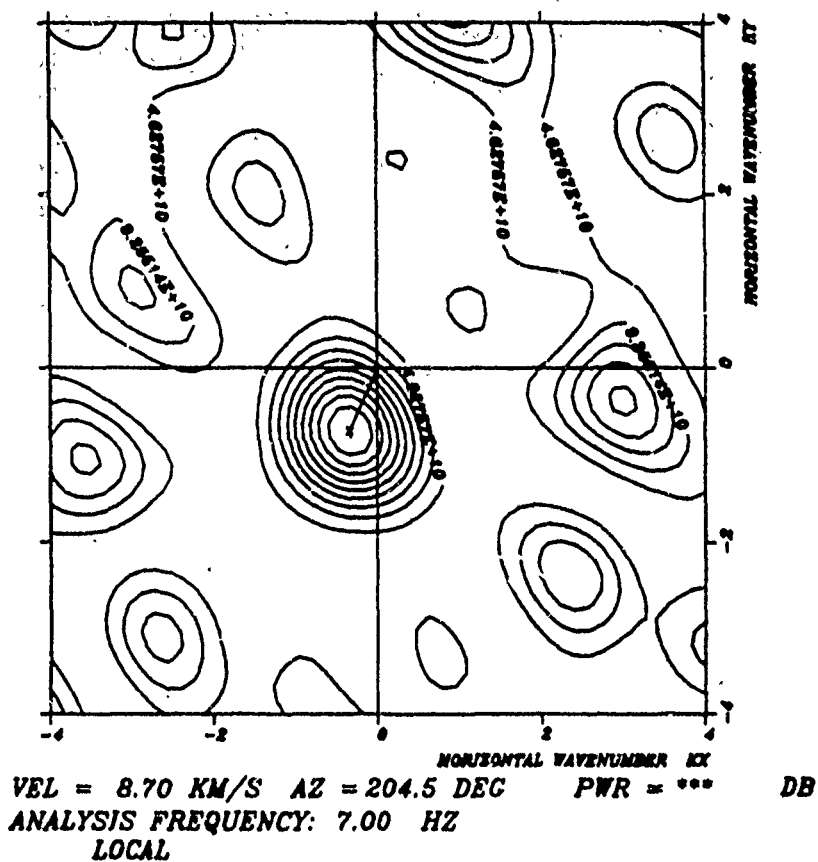


Figure 14. Frequency-wavenumber spectrum of event and window of figure 9 at a frequency of 7.2 Hz using subarray B.

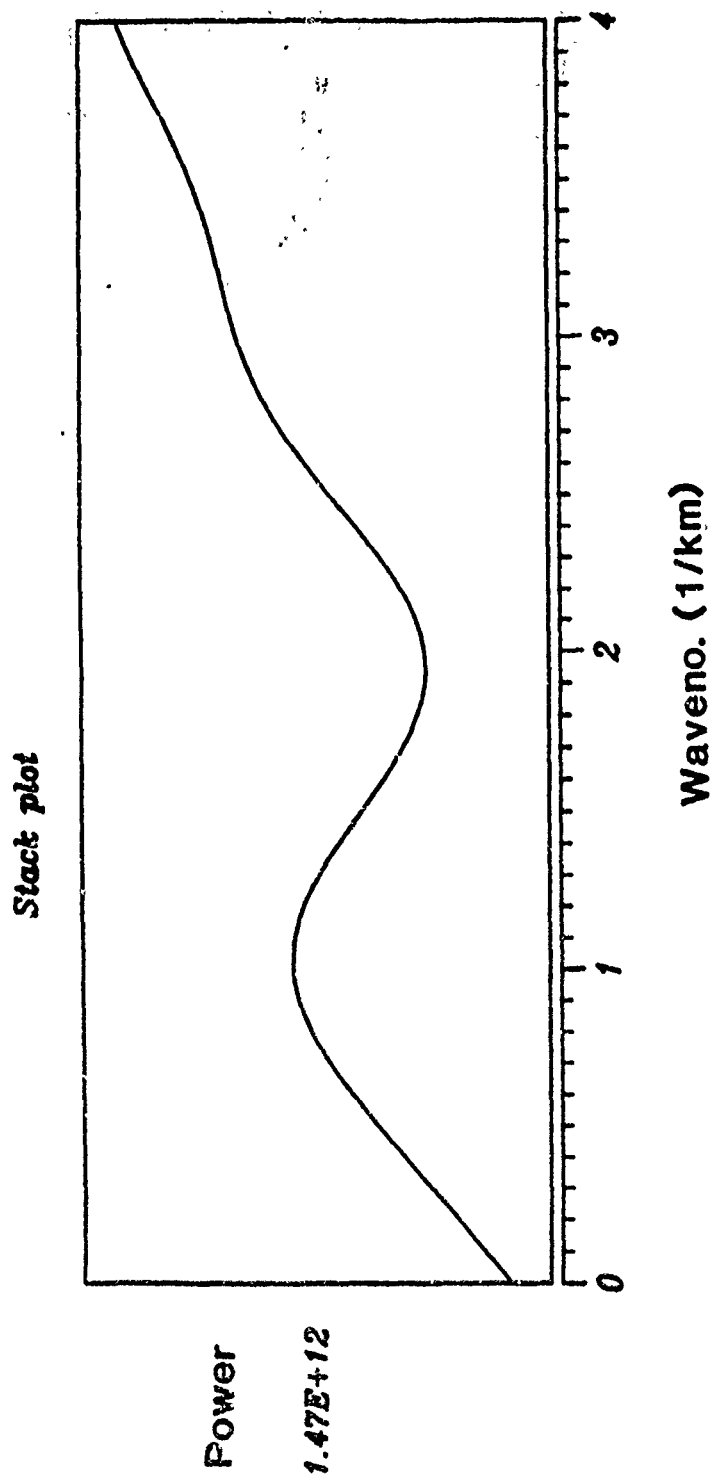


Figure 15. Wavenumber spectrum of event and window of Figure 9 at a frequency of 7.2 Hz using subarray B.

at a wavenumber of 2.4 km^{-1} (apparent velocity 3 km/s; Figure 13) that is not evident on Figure 15 (subarray B).

The peak at 2.4 km^{-1} appears to be an artifact caused by the sidelobe pattern of subarray A; a similar peak is seen on Figure 11 using the full array. Figures 16 - 18 show the beam patterns for, in order, the full array, subarray A, and subarray B. Figures 16 and 17 (the full array and subarray A) have the first sidelobes at wavenumbers of 1.9 km^{-1} from the central peak, while Figure 18 (subarray B) has the first sidelobes at 3 km^{-1} . These differences reflect the smaller aperture and the smaller average distance between seismometers of subarray B. Because the sidelobes are closer to the main peak for the full array and subarray A, spurious peaks due to the sidelobes will appear at lower wavenumbers than for subarray B. This is a potentially serious difficulty when searching for the diffuse coda components mentioned previously. In assessing the severity of the problem, note that the lowest apparent velocity of interest is 3 km/s and that the wavenumber corresponding to this may be calculated from (2) at any given frequency. If the full array or subarray A are to be used this maximum wavenumber should be $\leq 2 \text{ km}^{-1}$, while for subarray B the maximum wavenumber should be $\leq 3 \text{ km}^{-1}$.

The problem of bias in the velocity determination using wavenumber spectra has been examined through the use of synthetic data. Figure 19 shows a synthetic signal for the center seismometer of the array. A similar signal was placed on the other seismometers of the (full) array with the appropriate time shifts for a P wave coming from due North with an angle of incidence of 15° to the vertical. A surface velocity V_s of 6 km/s was assumed, corresponding to an apparent velocity V_a of 23.2 km/s, and a frequency of 2 Hz. Figure 20 shows the frequency-wavenumber spectrum; the correct velocity and azimuth are reproduced in the position of the peak. Figure 21 shows the wavenumber spectrum. The peak occurs at a wavenumber of 0.18 km^{-1} corresponding to a velocity of 11 km/s, confirming the bias suggested previously. This bias is caused by the spreading of the peak in the frequency-wavenumber plot due to the finite array aperture combined with the

THEORETICAL BEAMPATTERN
LINEAR DEPENDENCE BETWEEN CONTOURS

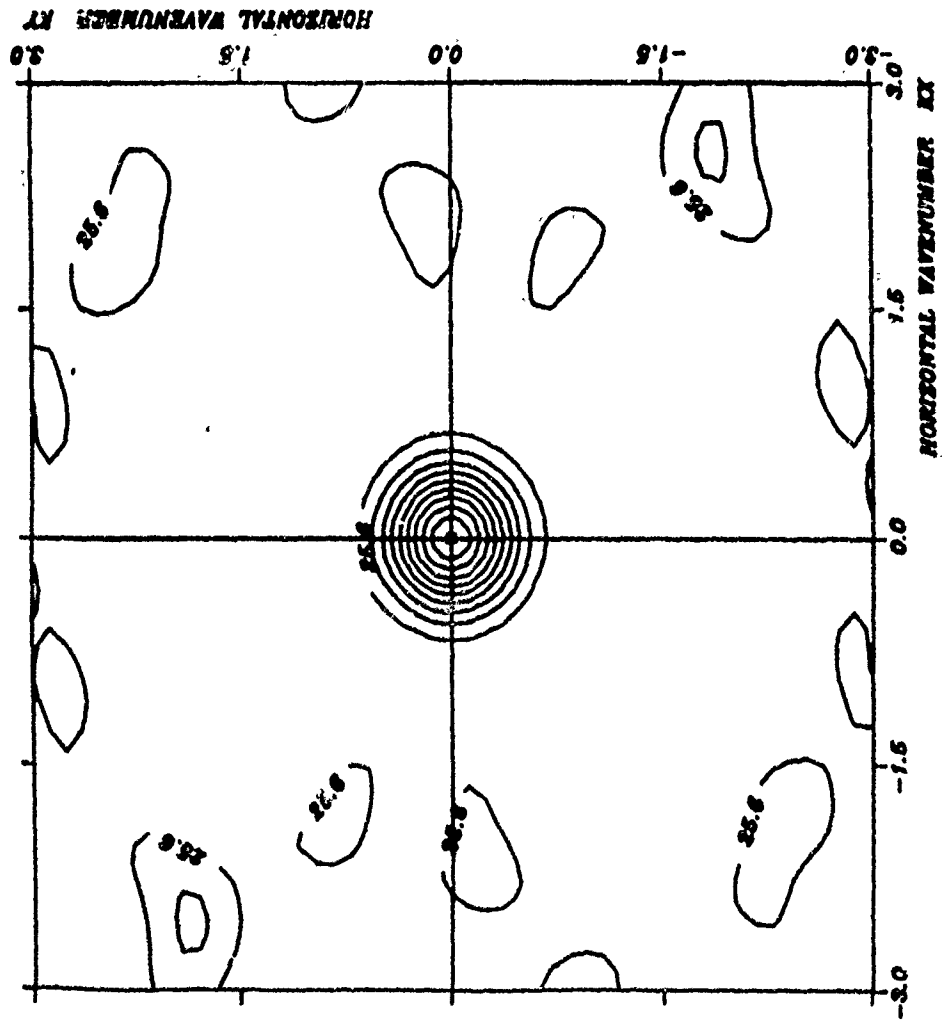


Figure 17. Beam pattern of subarray A.

THEORETICAL BEAMPATTERN
LINEAR DEPENDENCE BETWEEN CONTOURS

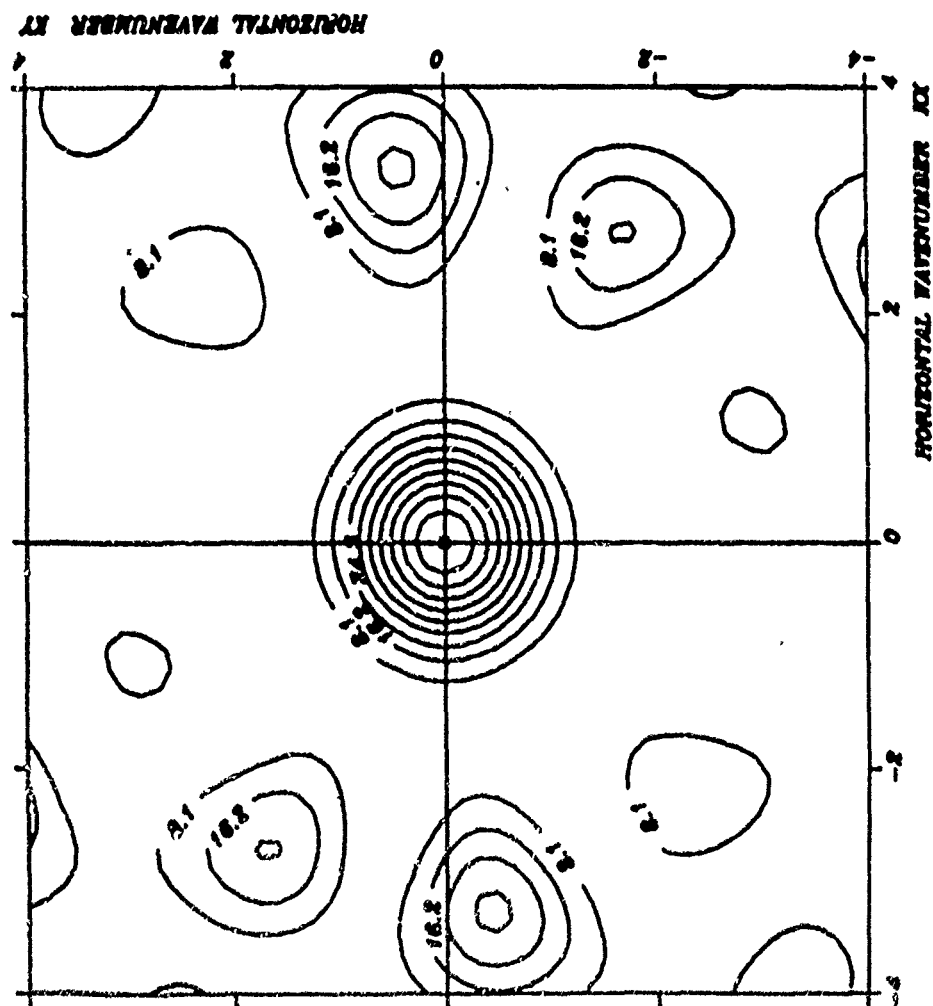


Figure 18. Beam pattern of subarray B.

SYNTHETIC 2 HZ

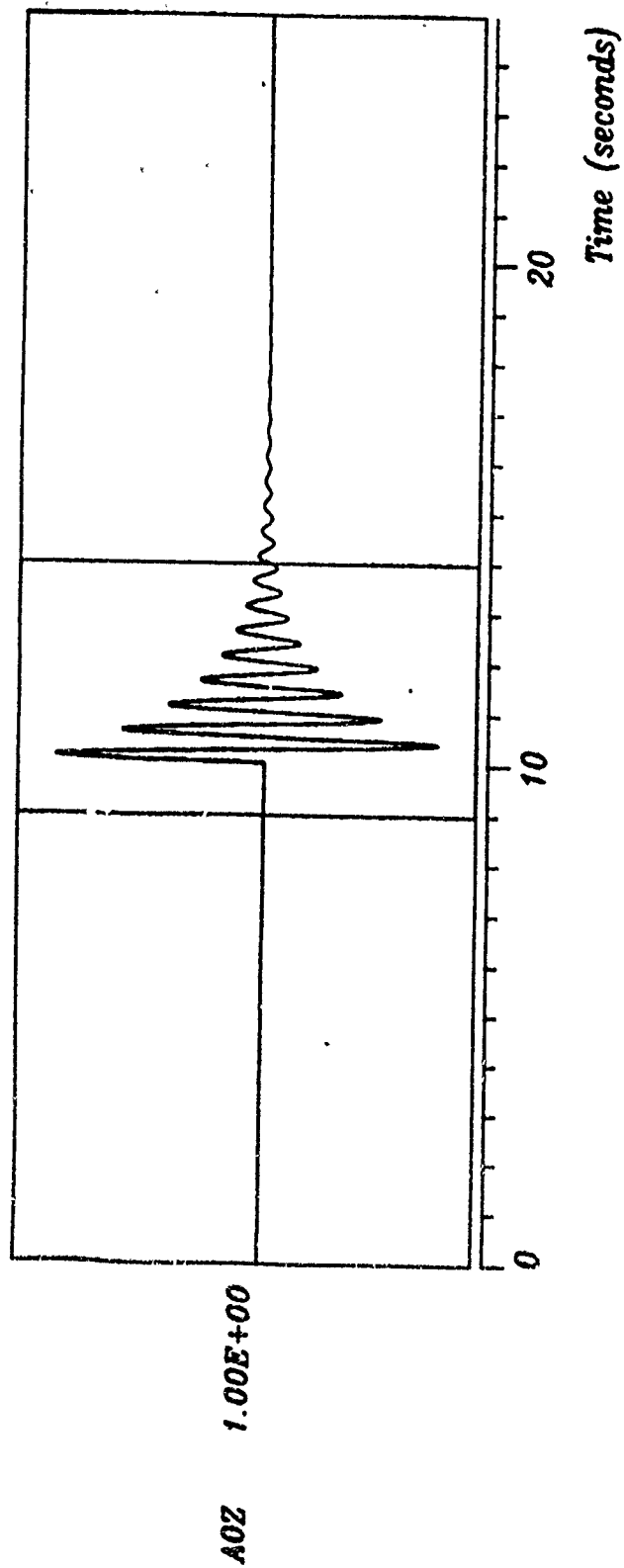


Figure 19. Synthetic signal of frequency 2 Hz applied to the center seismometer of the NORESS array. Analysis window indicated. See text for discussion.

MONOCHROMATIC F-K ANALYSIS
CONVENTIONAL RESOLUTION
LINEAR DEPENDENCY BETWEEN CONTOURS

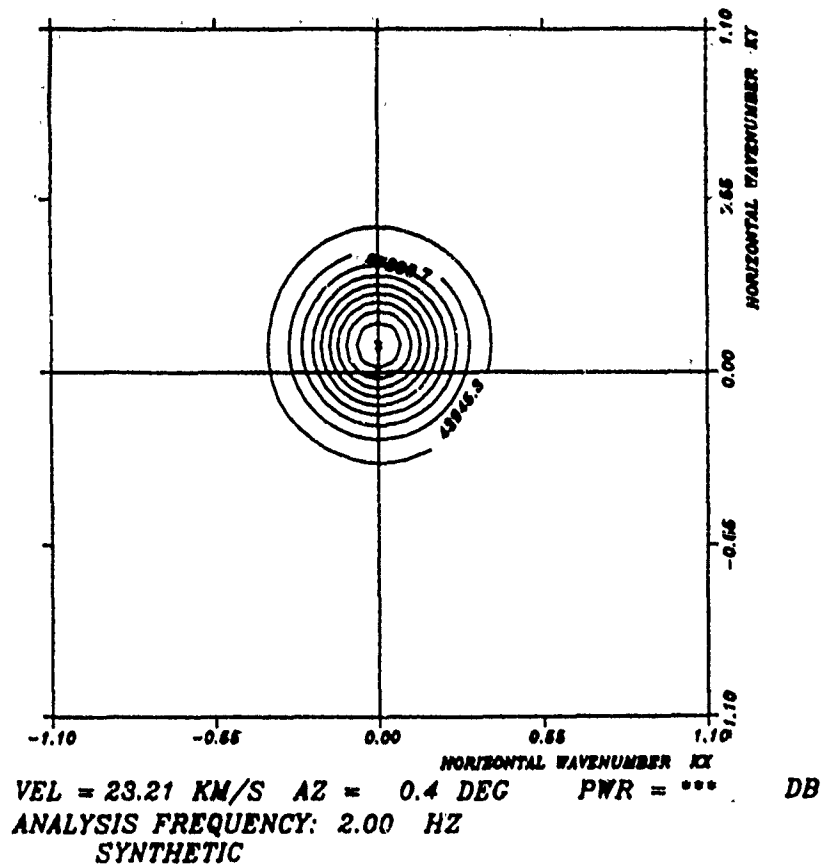


Figure 20. Frequency-wavenumber spectrum of signal and window of Figure 19 at a frequency of 2 Hz using full array.

SYNTHETIC 2 HZ 23 KM/S

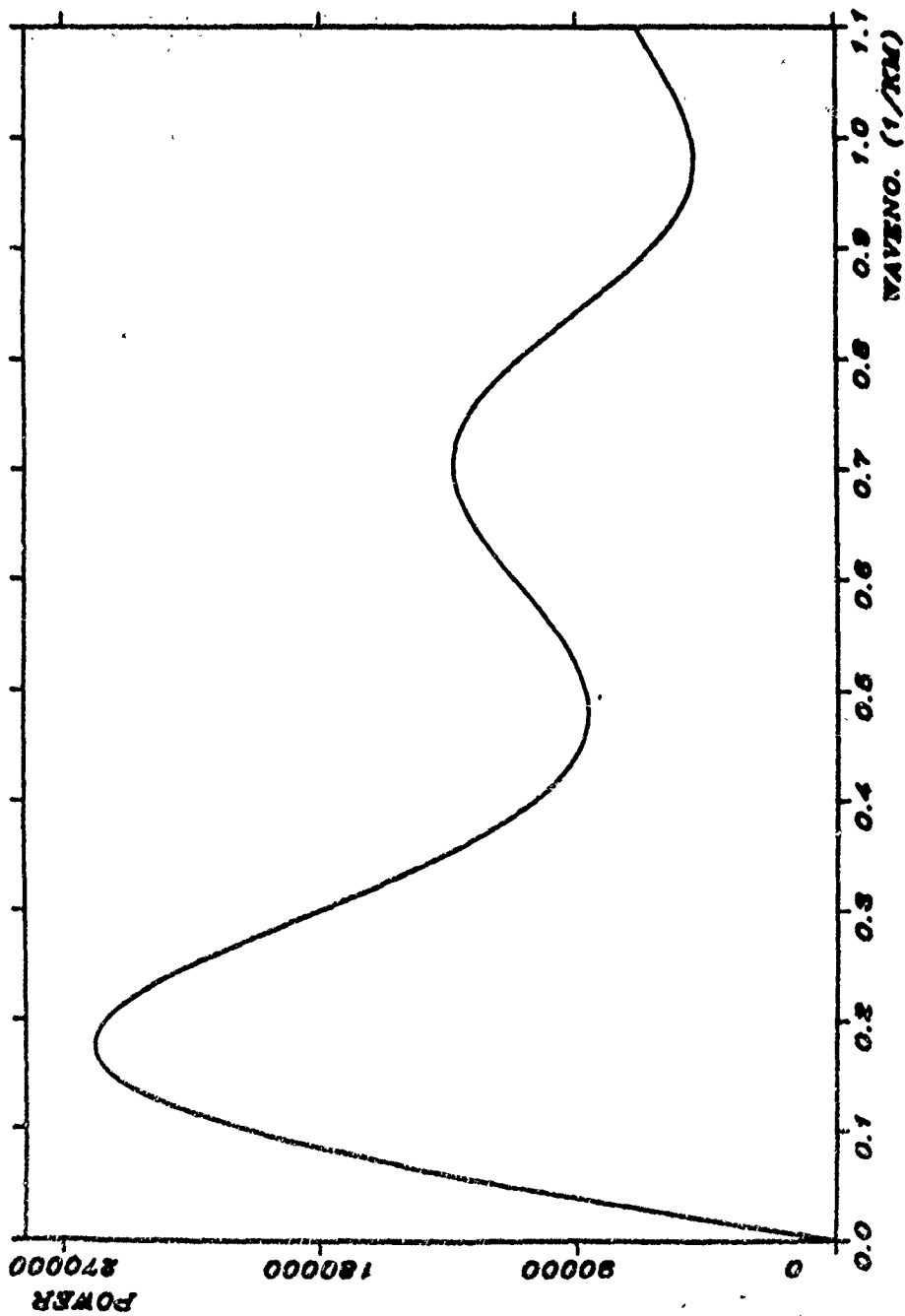


Figure 21. Wavenumber spectrum of signal and window of Figure 19 at a frequency of 2 Hz using full array.

increasing circumference of the circle of integration, which tends to weight larger wavenumbers disproportionately, especially if the broadened peak overlaps the origin of the frequency-wavenumber plane.

The effect described above has been evaluated by repeating the experiment shown in Figures 19 - 21 for frequencies of 1 and 2 Hz and true apparent velocities from 2.0 to 23.2 km/s. Results are presented in Figure 22, which plots the measured velocity using the wavenumber spectrum against the true velocity. Besides allowing us to estimate corrections to the measured velocity, Figure 22 demonstrates that there is a "saturation" phenomenon at high velocities - for 1 Hz, the maximum value of the measured velocity is 5.9 km/s by this method, no matter how fast the true velocity. Let the horizontal wavelength be defined as

$$\lambda = 1/k = V_a/f \quad (6)$$

This wavelength describes the length scale of the wave as viewed by the array. If the bias is due to the finite array aperture, we would expect some measure of the bias such as the ratio R of the measured to the true velocity to depend only on the ratio of λ to the array aperture A . In Figure 23 the results shown in Figure 22 are replotted as a graph of R against λ/A . The points for 1 and 2 Hz both fall on the same curve, indicating that the bias is indeed controlled by array aperture. The curve falls between two asymptotes, $R = 1$ for $\lambda/A \rightarrow 0$ and $R = 2/(\lambda/A)$ for λ/A large. The second asymptote expresses the saturation effect described above.

The results of the investigations into bias have a number of practical implications for work on coda. Corrections to observed velocities may be made using the information presented in Figures 22 and 23. The most convenient method of doing this is Figure 24, which plots R against λ'/A , where λ' is measured by substituting the measured velocity for the true velocity in (6). The high wavenumber saturation asymptote becomes $\lambda'/A = 2$. Another important result of the bias study is the finding that it is not possible to measure velocities faster than a certain limit for a given combination of array aperture and

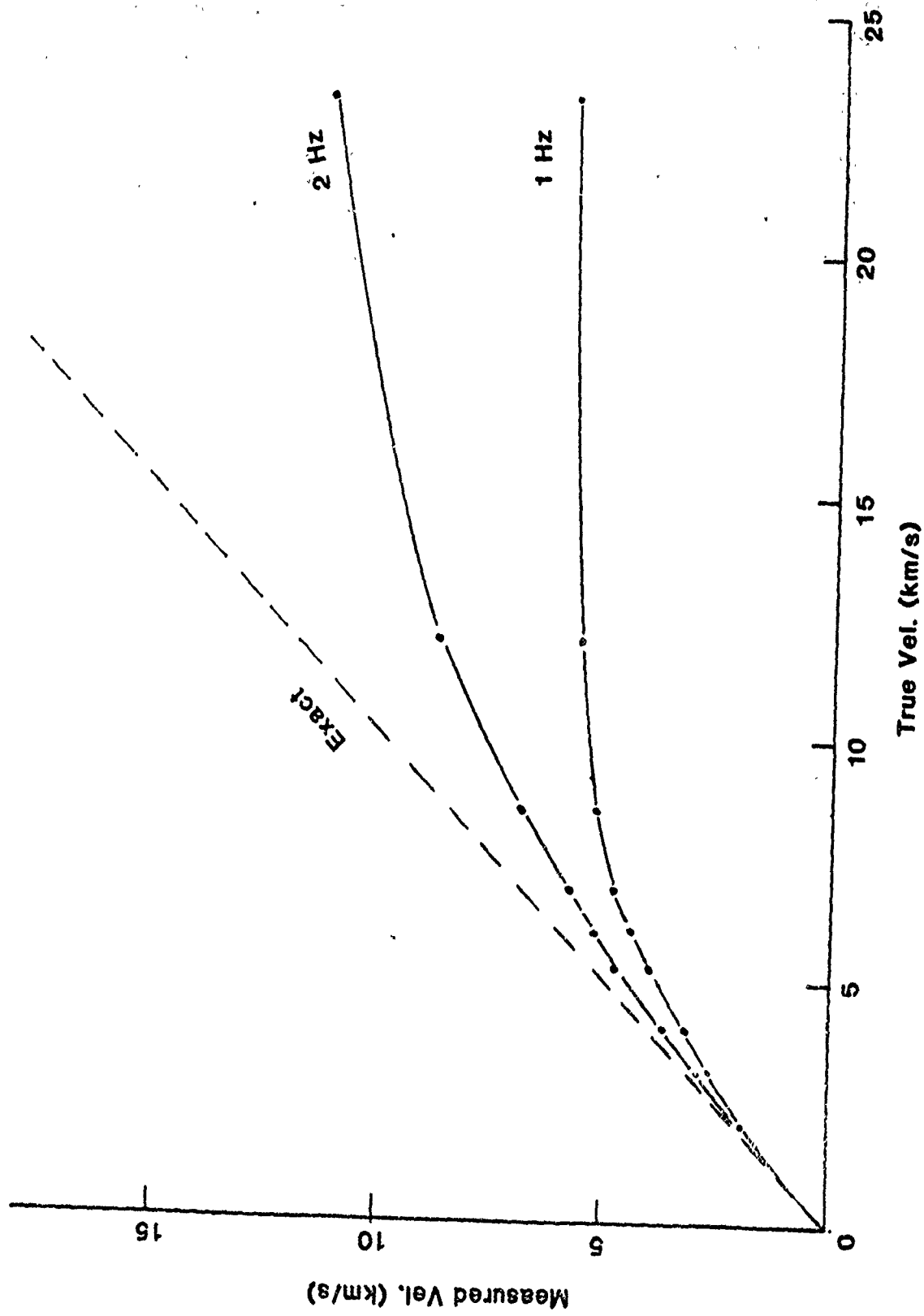


Figure 22. Measured velocity using wavenumber spectra and full array plotted as a function of true velocity for synthetic signals of 1 and 2 Hz.

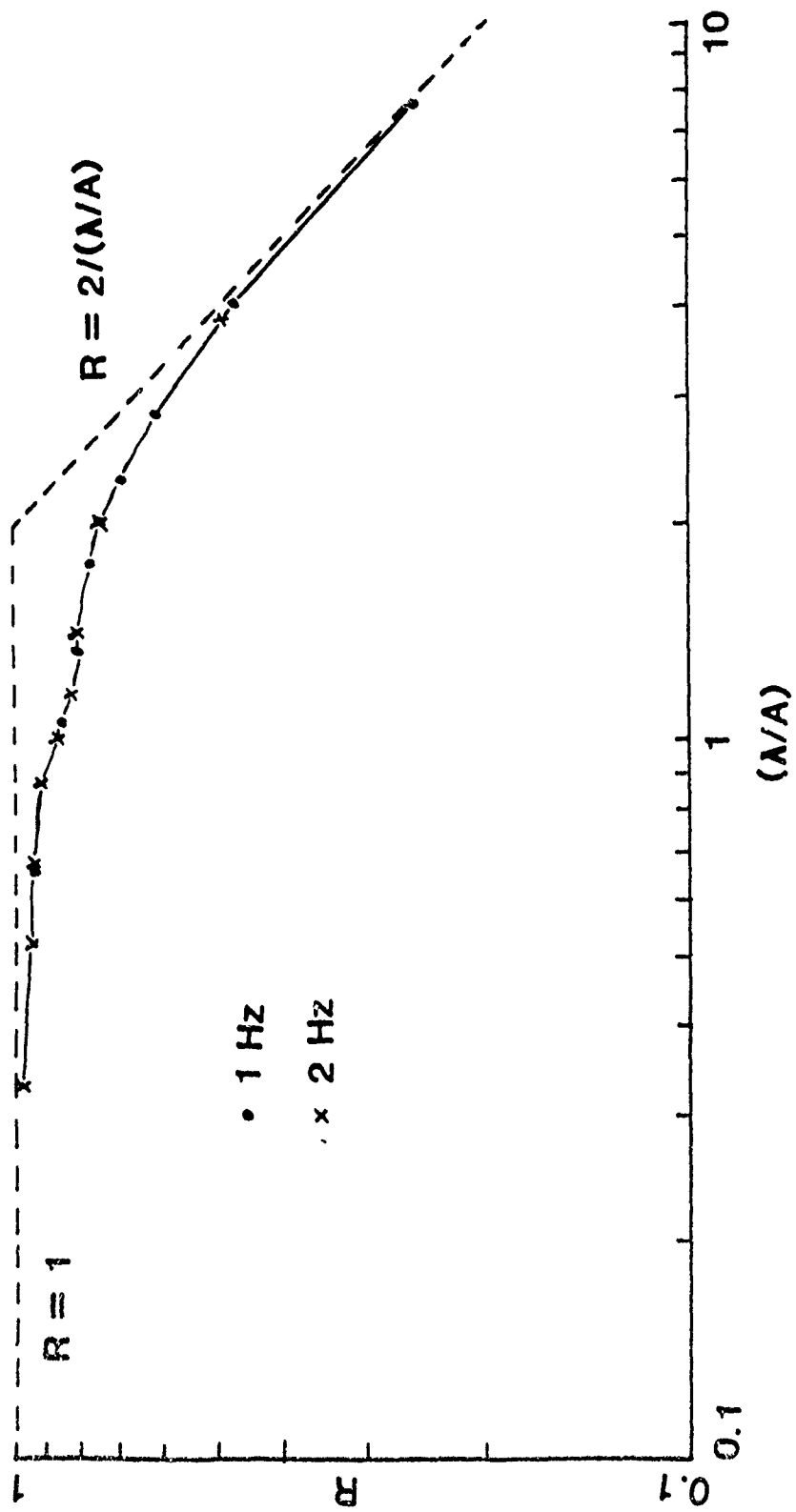


Figure 23. Data of Figure 22 replotted as R against λ/A . See text for discussion.

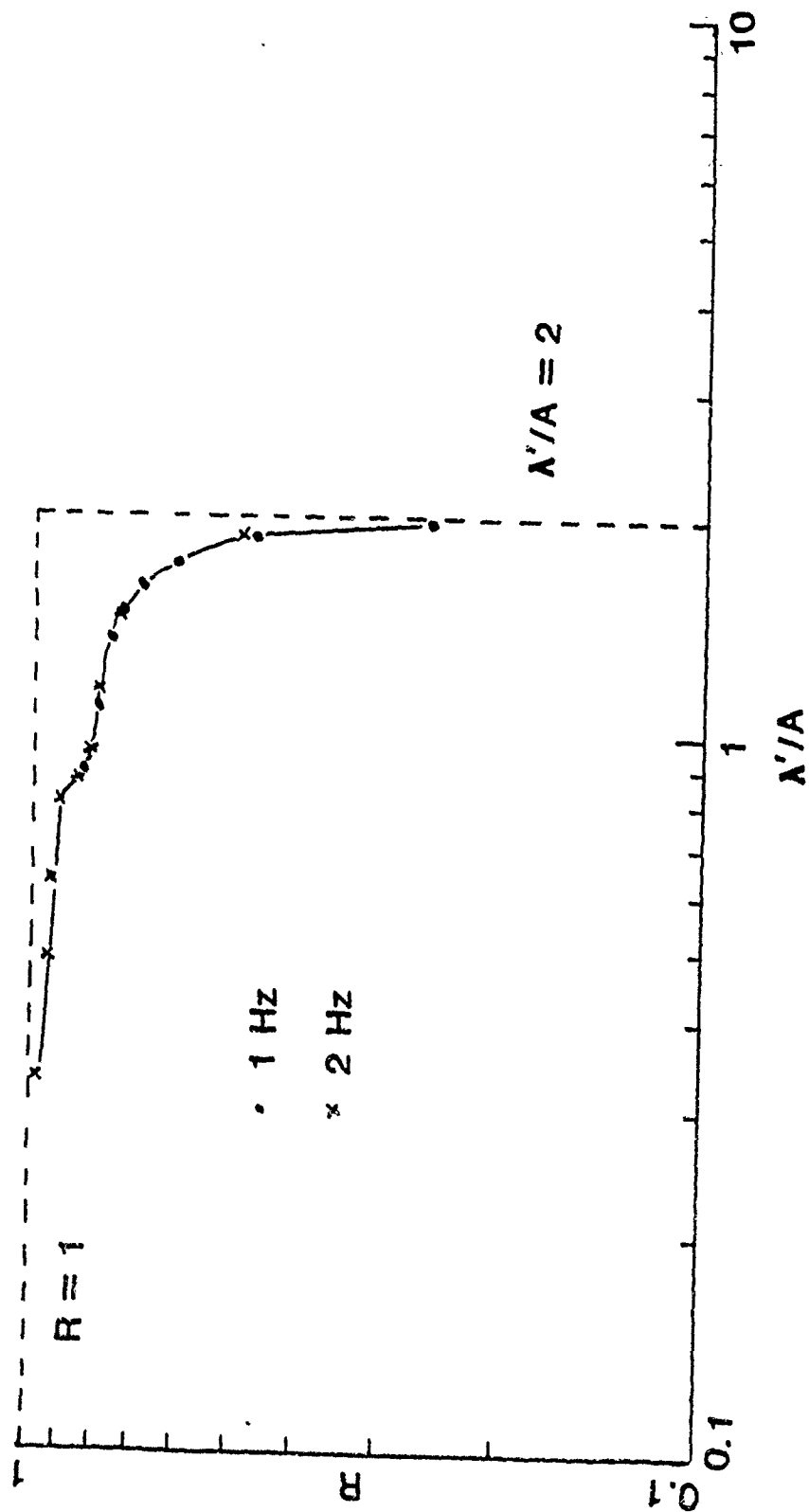


Figure 24. Data of Figure 22 replotted as R against λ'/A . See text for discussion.

frequency. The practical limits are $\lambda/A = 2$ or $\lambda'/A = 1.5$, with the velocities then determined through (6). At 1 Hz with the full array, for example, this leads to a (true) velocity limit of 6 km/s, meaning that it is possible to distinguish between S waves and P waves but not between crustal P and teleseismic arrivals. This is probably the minimum requirement for a useful array.

The final step in this investigation is the setting of frequency bands within which different array configurations should be used. The problems of coherence and sidelobe interference demand as small an array as possible, while minimization of velocity bias requires as large an aperture as possible (the aperture of the full array is 3 km, of subarray A 1.5 km, of subarray B 750 m). A minimum velocity limit of 6 km/s, as discussed in the last paragraph, is used to determine the aperture. Then the following combinations of frequency and array configuration are proposed: 1 - 2.5 Hz, the full array; 2.5 - 5 Hz, subarray A; 5 - 10 Hz, subarray B. Wavenumber spectra should not be used for frequencies less than 1 Hz at NORESS. Note that the investigations of Dainty (1985) using the full array in the frequency range 1 - 2 Hz meet the recommendations given above.

III. ULTRASONIC MODELLING

This section gives a very brief report of ultrasonic investigations into coda. At this stage, a particular target is the testing of the single backscattering theory of the coda advanced by Aki (1969) and Aki and Chouet (1975). This theory has become the standard model of the coda and forms the basis of the measurement of attenuation and magnitude using coda, an increasingly important endeavour. In spite of this, there has been no good test of the single scattering assumption, a crucial point in the theory. Dainty *et al.* (1984) suggest that in several cases of local earthquake codas examined the assumption of single scattering was violated. Accordingly, it is proposed to test the single backscatter theory of local coda by constructing two dimensional ultrasonic models consisting of 1/16" aluminum plates with holes or other shapes drilled into them as scatterers.

As a first step one such plate has been constructed (Figure 25). The (identical) transducers are small (~ 2 mm diameter) piezoelectric crystals; orientated as shown in Figure 25 they will produce and record motions transverse to the plate, corresponding to flexural modes. Flexural modes show pronounced dispersion if the wavelength is greater than six (6) times greater than the plate thickness but travel at close to the shear wave speed for shorter wavelengths (Ewing *et al.*, 1967, p. 285), with motion predominantly transverse to the plate. For wavelengths less than six times the plate thickness, flexural modes may be a good two dimensional analog of SH. This has the advantage of making interpretation of the results simpler because SH does not convert to P or SV upon reflection or scattering. Figure 26 shows a seismogram taken using the setup in Figure 25. The dominant frequency is about 500 kHz; since the velocity of shear waves in aluminum is 3 mm/ μ s, the wavelength is 6 mm, meeting the criterion for SH motion; dispersion is not evident. This conclusion is supported by the travel time of the dominant arrival in Figure 26, 30 μ s after origin, appropriate for a shear wave travelling 90 mm (Figure 25). Some P energy is visible before this time, but it is small. We have confirmed that there is little motion parallel to the plate. Figure 26 may be compared with a local earthquake seismogram, Figure 27 (from

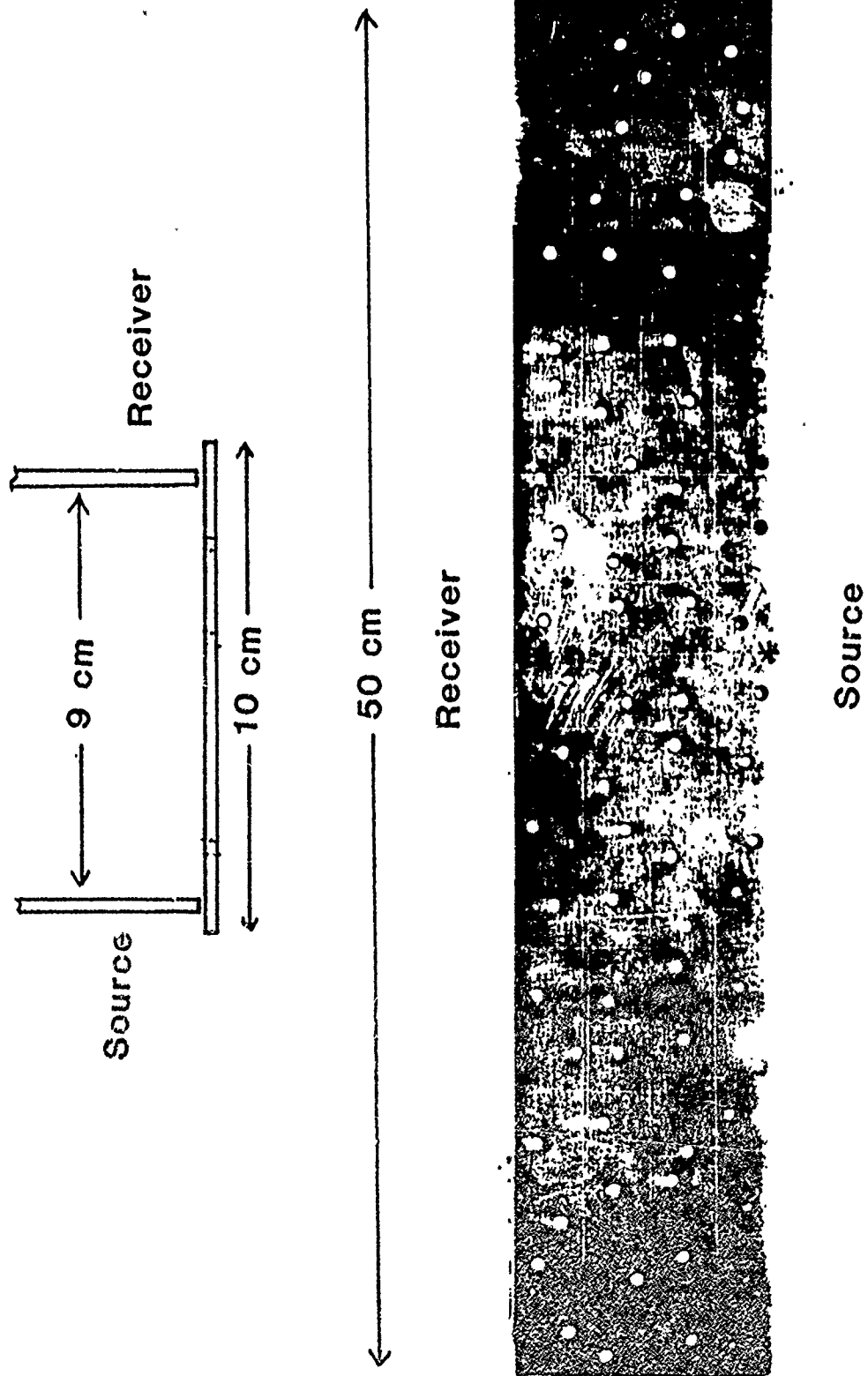


Figure 25. Ultrasonic model for coda. (Top) Section view showing orientation of sensors. (Bottom) Plan view.

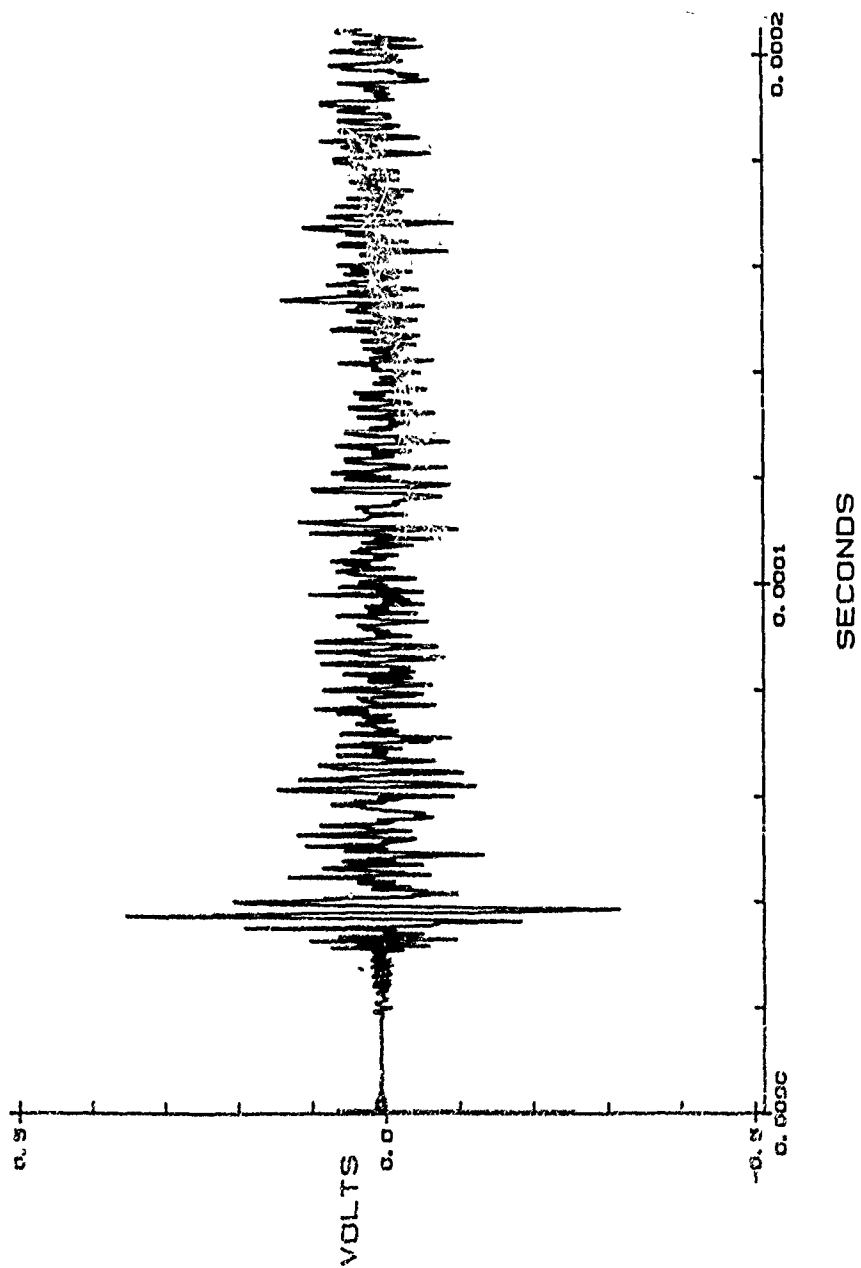


Figure 26. Recording made using setup of Figure 25. Total length of time axis is 200 μ s; time 0 is the time of source firing.

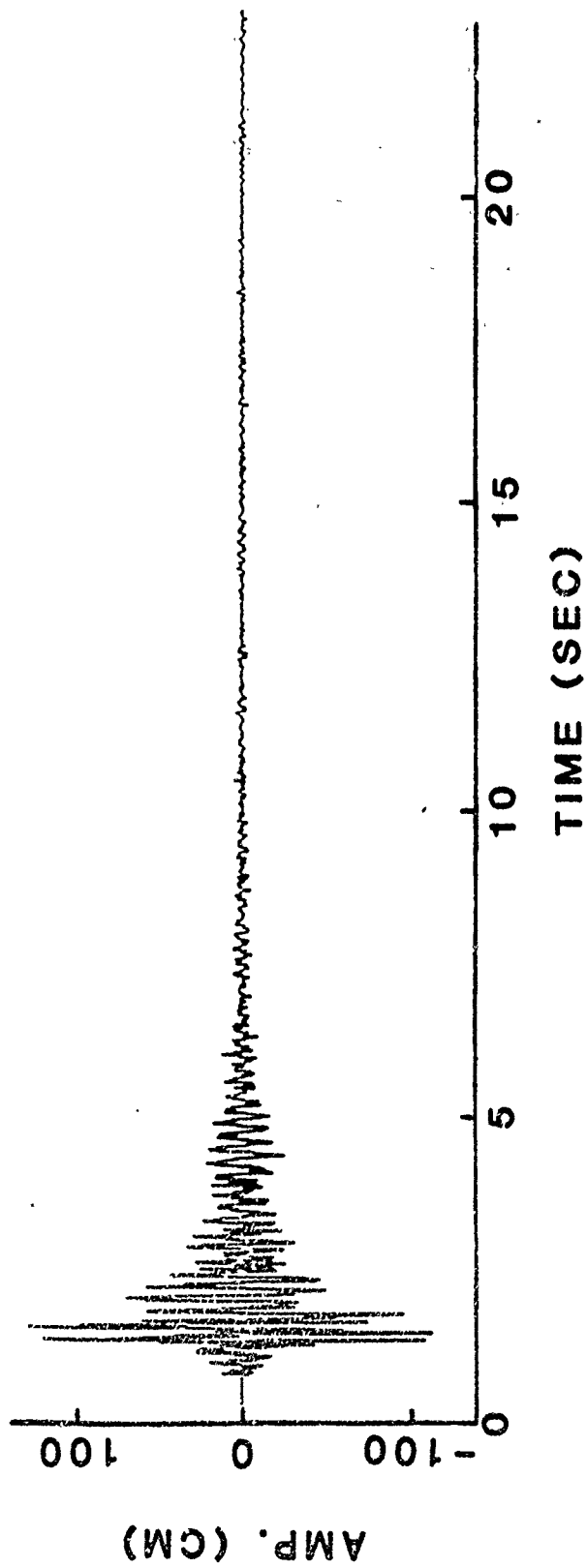


Figure 27. Local earthquake seismogram recorded at Monticello, SC. From Dalnity *et al.* (1984).

Dainty *et al.*, 1984).

The final consideration in constructing the model is the matter of scaling between the earth and the model. Obviously, the model is much simpler than the earth, but some scaling considerations still apply. Since the shear velocity of the crust is about the same as aluminum (3 km/s), wavelengths scale inversely as frequencies; thus 5 Hz waves in the crust, a typical case from Dainty *et al.* (1984), will be equivalent to 500 kHz waves in the model if km in the earth correspond to cm in the model. In the model shown in Figure 25, the scatterers (holes) are 5 mm (about one wavelength) across and correspond to objects of about 500 m linear dimension in the earth, although they are almost certainly stronger scatterers than found in the earth. Another important factor in the scaling is the length of the plate, since this controls how far waves travel (50 cm) before they can contaminate the coda due to end reflections. This implies that the coda is uncontaminated by end reflections before 170 μ s, i.e., most of the record shown in Figure 26. This scales to codas up to 17 s after origin in the earth, covering many of the codas considered in Dainty *et al.* (1984).

The second quantity that has to be scaled is the mean free path, which is the reciprocal of the total turbidity. Dainty *et al.* (1984) found mean free paths between 10 and 100 km; scaling this to the model (10 - 100 cm) means that codas containing scattered waves that have traversed 0.5 - 5 mean free paths may be investigated. This appears to be the interesting range. To achieve this, the number, type and shape of scatterers will be varied as well as the ultrasonic frequency and the length of the plate. A particular object of study will be the transition from single to multiple scattering and its effect on parameters derived from the coda.

REFERENCES

- Aki, K. (1969). Analysis of the seismic coda of earthquakes as scattered waves. *J. Geophys. Res.* 74, 815.
- Aki, K. and B. Chouet (1975). Origin of coda waves: source, attenuation and scattering effects. *J. Geophys. Res.* 80, 3322.
- Bullitt, J. T. and V. F. Cormier (1984). The relative performance of m_b and alternative measures of elastic energy in estimating source size and explosion yield. *Bull. Seis. Soc. Am.* 74, 1863.
- Bungum, H., S. Mykkeltveit and T. Kvaerna (1985). Seismic noise in Fennoscandia, with emphasis on high frequencies. *Bull. Seis. Soc. Am.* 75, 1489.
- Dainty, A. M. (1985). Coda observed at NORSAR and NORESS. Final Report AFGL-TR-85-0199, ADA166454.
- Dainty, A. M., R. M. Duckworth and A. Tie (1984). Influence of scattering on Q in the lithosphere. Final Technical Report, Contract AFOSR-83-0037.
- Ewing, M., W. S. Jardetzky and F. Press (1957). *Elastic Waves in Layered Media*. McGraw-Hill, New York, New York.
- Gupta, I. N., R. R. Blandford, R. A. Wagner, J. A. Burnett and T. W. McElfresh (1985). Use of P coda for determination of yield of nuclear explosions. *Geophys. J. Roy. Astr. Soc.* 83, 541.